Numerical Investigation of Pneumatic Flap Based on Circulation Control Technology

WANG Ruiwen[1], HUANG Xudong[1]

[1] Tsinghua University, Beijing 100084, China
xdhuang@tsinghua.edu.cn

Abstract. Circulation control technique induces deflection of the airflow near the wing and changes the aerodynamic forces and moments to achieve the purpose of attitude control of the aircraft normally. It could generate virtual rudder surfaces through the Coanda effect caused by high-speed jets at the trailing edge of the wing. Since the monoplane geometry could not be optimal for all conditions encountered, circulation control technique, used at the trailing edge of the wing, replaces the existing high-lift flaps and control surfaces to modify the shape of the wing during takeoff and landing as well as cruise of the aircraft, so that the wing could be continuously deformed to its optimal pressure distribution state according to specific conditions. For this purpose, in this paper, numerical simulation of CC-E0020EJ, which is large thickness symmetric airfoil, and supercritical circulation control airfoil (GACC) has been carried out using CFD++. The flow field analysis of the two circulation control airfoils is performed by changing the jet momentum coefficient to determine the control ranges of the maximum lift coefficient and the maximum lift-to-drag ratio. In this paper, the aerodynamic shape optimization is accomplished by using the circulation control, and the virtual flaps formed by the high-speed jet provide a method to determine the optimal wing shape equivalent curvature in order to achieve the ideal control effect of pitching moment under different flight conditions. The high-speed jet separated from the trailing edge of the wing to form an aerodynamic flap can change the equivalent curvature of the wing, which makes the forward stationary point move backward and the trailing edge separation point move downward on the curved surface, forming a control effect similar to that of a variable curvature airfoil.

Keywords: Circulation control, Coanda effect, Moment control.

1 Introduction

For a long time, the high lift characteristics of fixed-wing aircraft have been provided by different wing geometries, often employing methods such as leading and trailing edge flaps, variable camber airfoils, or active flow control to enhance the aerodynamic performance of the wings. In conventional aerodynamic design, even with multi-point multi-objective optimization, fixed-wing aircraft can only to a limited extent balance the lift-to-drag performance beyond the design point, and the lift-to-drag ratio deviates from its optimum value after departing from the cruise design point. As the modern

aircraft demand higher lift-to-drag characteristics and maneuvering force moments, the performance requirements of fighter jets and transport planes have surpassed the limitations imposed by the geometric configurations of fixed-wing wings. In this context, active flow control technology has gained considerable attention from the industry.

As a classic active flow control technique, circulation control involves introducing secondary jets to alter the local or global flow around an aircraft, generating the required aerodynamic forces and moments for flight control. This technology creates a "virtual control surface" effect similar to mechanical control surfaces, simultaneously enhancing lift-to-drag ratios and modifying flow field characteristics according to flight conditions, thus offering a flight control approach that balances high lift and enhanced maneuverability. International researchers began exploring circulation control techniques as early as 1962[1], with various research institutions subsequently conducting prototype validation efforts. BAE Systems, UK, unveiled the DEMON[2] and MAGMA[3] unmanned aerial vehicles in 2010 and 2017 respectively, pioneering demonstrations of jet-driven flight control integration. NATO Science and Technology Organization (STO)[4][5][6] initiated evaluations of active flow control techniques, including trailing-edge circulation control, starting in 2013. Institutions like Nanjing University of Aeronautics and Astronautics in China [7][8][9] initiated fundamental studies and flight test research. The unmanned aircraft α-31, co-developed by a team led by CAE[10][11], underwent flight demonstration validations in 2018 and 2019. In 2021, the team led by Luo Zhenbing from the National University of Defense Technology[12] achieved the first lateral crosswind flight control experiment without traditional control surfaces.

Historically, researchers have often regarded circulation control as a means to achieve increased lift, extensively analyzing various 2D wing profiles and flight conditions. For the NACA0012 airfoil, Zhang Weiwei[13] et al. designed a high-frequency low-power synthetic jet actuator on the trailing edge to study the unsteady aerodynamic characteristics of side and upper jets using wind tunnel experiments. Liu Xiaobo[14] et al. conducted numerical simulations on the NACA0012 airfoil with this synthetic jet actuator installed at zero angle of attack. Zhang Zhiyong[15] et al. employed Favre-filtered large eddy simulation to numerically simulate suction and blowing jets on the upper surface of the NACA0012 airfoil. Yonghong Li[16] et al. investigated blowing on the lower surface of the NACA0012 airfoil and completed unsteady numerical studies on arbitrary-shaped gust loading. Li Yujie[17] et al. designed a horizontal synthetic dual-jet exciter for the mid-span of the NACA0015 airfoil, studying full separation at high angles of attack. Englar[18] and team examined NASA's Cruise Efficient Short Takeoff and Landing (CESTOL) project, developing CC020-010EJ for supersonic aircraft's lift and cruise performance enhancement using CFD and experimental verification. For multi-segment wings, Bai Junqiang[19] et al. increased flap angles on the basis of L1T2 multi-segment wing models, studying zero-mass jet and distributed zero-mass jet. Han Zhonghua[20] and team analyzed dynamic stall control effects of the OA212 helicopter rotor airfoil. Yang Xiaoguang[21] et al. studied Lockheed Georgia's circulation control wing (CCW-LG), comparing performance for various trailing edge shapes. Jiang Yubiao[22] et al. explored the time-dependent characteristics of a GTRI double-arc circulation control airfoil with a maximum thickness of 16% chord length. Kong

Bo[23] et al. designed airfoil profiles for two-dimensional seamless deflection, achieving high lift through trailing edge jets. Regarding supercritical airfoils, Lei Yuchang[24] and team numerically simulated GACC (Georgia Institute of Technology Adaptive Compliant Compressor) forced pitch oscillations on the NASA LS (1)-0417 supercritical airfoil, investigating unsteady lift and pitching moment characteristics at various momentum coefficients. Jone[25] et al. verified the steady and pulsating aerodynamic performance of the GACC airfoil using computational fluid dynamics and experiments. However, few studies have conducted comparative research on various airfoil profiles.Recent years have seen global research institutions focus on the application of circulation control technology to aircraft. Wang Lei[26] et al. analyzed lift enhancement and roll performance of the Clark-Y airfoil using unsteady simulations, concluding that circulation control delays stall angle, increases maximum lift coefficient by up to 32.4%, and achieves roll moments superior to 30° deflection of control surfaces. George Hoholis[27] studied the CC0020 circulation control airfoil and SACCON unmanned aerial vehicle, followed by numerical simulations exploring pitch and roll moments controlled by trailing-edge momentum on unmanned aircraft.

Existing research primarily discusses the principal mechanisms of two-dimensional circulation control airfoil profiles across various geometries, summarizing regularities under low-speed flight conditions, yet the exploration of three-dimensional aircraft effects remains insufficient. This study is conducted in two stages. In the first phase, a comparative analysis is performed on the aerodynamic flap effect formed by two-dimensional thin airfoil profiles under high-speed jets, investigating the control range of circulation control technology. By adjusting the surface pressure distribution through jet blowing rate variation, changes in the lift coefficient for different jet blowing rates and angles are studied. In the second stage, a three-dimensional swept-wing model is established and numerically simulated. Considering the distinct flow field distribution for different sweep angles, the influence of wingtip vortices on trailing-edge jets is determined based on pressure distribution on the three-dimensional wing surface and the range of influence of wingtip streamlines. Subsequently, jet positions with minimal wingtip interference are defined, and the wing with different swept-back angles is investigated. Prior research considered full aircraft layouts and emphasized adding trailing-edge jets to a fixed wing layout, aiming to rationalize lift distribution and optimize attitude control. However, the important factors investigated in this study, such as the 2D equivalent camber, jet exit deflection, and 3D wingtip vortex interference, were not observed or at least not extensively described. Such flow phenomena are not observable within the confines of research focusing solely on individual fixed-wing configurations.

2 Numerical Simulations

Takeoff performance of different airfoils is selected as the object of study, and airfoils with different thicknesses and curvatures are analyzed. In order to ensure the reliability of the results of the calculation and analysis, the calculation adopts CFD++ for numerical simulation and analysis. Considering the influence of the high-speed jet from the

trailing edge nozzle on the aerodynamic characteristics of the wing, the force measurement method of push-resistance decomposition is adopted, and the computational analysis method selected in this paper is verified and analyzed.

According to the definition of ring volume and Kutta–Joukowski theorem, it is known that by increasing the surface velocity of the airfoil and increasing the gas flow trajectory the ring volume of the airfoil can be increased and the lift can be improved.

$$\Gamma = \mathrm{VdL} \tag{1}$$

$$Y = \rho V_{\infty} \Gamma \tag{2}$$

Wide range of researchers have indicated that the momentum coefficient is an important parameter affecting the Coanda effect, and that the lift force is strongly influenced by the momentum coefficient, which is defined as the projectile momentum coefficient:

$$C_{\mu} = \frac{\dot{m}}{q_{\infty} S} = \frac{\rho_J U_{jet}^2 A_J}{q_{\infty} S} \tag{3}$$

Where $\dot{m}$ represents the mass flow rate of the jet; U_{jet} represents the velocity of the jet; S represents the reference area of the experimental model, i.e., the chord length c; AJ represents the area of the jet nozzle per unit of spreading length, i.e., the height of the jet nozzle h; qœ represents the incoming flow pressure; and Cμ denotes the ratio of the jet flow flux to the free stream flow flux.

2.1 Numerical Method

In this paper, the Navier-Stokes (RANS) equation solver is used to perform constant state simulation. It is crucial to correctly choose a turbulence model that reflects the characteristics of the flow field. High accurate turbulence models have been explored in previous studies, so this paper continues to follow the Realizable *k*-*ε* turbulence model for full turbulence calculations. The GACC airfoil based on NASA LS(1)-0417 supercritical airfoil modification and the standard circulation control airfoil CC-E0020EJ are selected to calibrate the solver accuracy. The GACC airfoil is calculated as follows: incoming velocity U_{∞}=30 m/s, Reynolds number Re=5.00×10^5. The CC-E0020EJ airfoil is calculated as follows: Mach number Ma=0.1, Re=2.3622×10^6, and jet moment coefficient C_{μ}=0.047. In order to eliminate the influence of the mesh and accurately capture the flow characteristics of the adhering surface layer, it should be ensured that the y+ value is between 0 ~1, ensure that the first node is located in the viscous sublayer, and calculate the heights of the first mesh layer of the object surface to be 4.84×10^{-5}m and 2.88×10^{-6}m, respectively.

The far-field boundary of the computational domain consists of an O-grid, and the radius of the wing far-field boundary is taken to be 15 *c*. Fig. 1. plots the 2D wing mesh topology and the mesh distribution near the object surface. The boundary conditions are set as follows: no-slip boundary condition is used for the object surface and pressure far-field boundary condition is used for the far-field. The calculated mesh volumes for the GACC and CC-E0020EJ wings are obtained as 76960 and 87084, respectively.

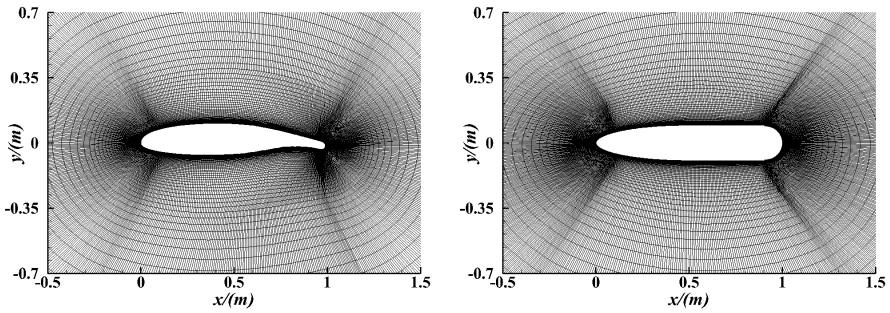

(a) GACC Airfoil (b) CC-E0020EJ Airfoil

Fig. 1. Airfoil mesh topology and object surface near the grid.

2.2 Verification of Numerical Methods

By comparing the GACC airfoil with the NASA experimental data[28], it is verified that high computational accuracy can be achieved under different jet momentum coefficients. Fig. 2. plots the lift coefficient curves of numerical computation and experimental results in the range of C_μ = 0~0.10. When the momentum coefficient C_μ is lower than 0.01, the prediction result of the lift coefficient is slightly lower than the experimental value, which is judged to be caused by the inconspicuous wall-attachment effect of the simulation results in the case of low-speed jets; when the momentum coefficient C_μ is higher than 0.04, the computed value of the GACC is on the large side, and according to the analyses of other researchers, the computed results of the CFD are usually over-predicting the wall-attachment effect of the jets and delaying the flow separation. To summarize, the trends of the lift coefficients versus jet momentum coefficients curves are quite consistent and can capture the separation control phase and the super circulation control phase more accurately.

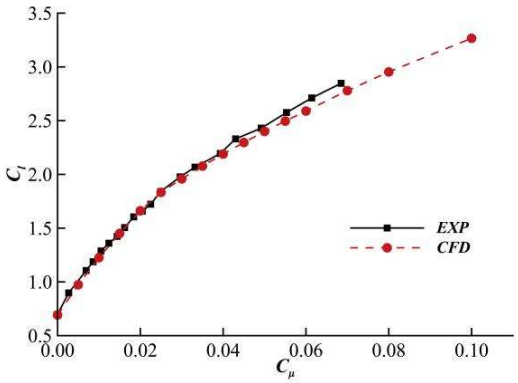

Fig. 2. Comparison of lift coefficients between numerical simulation and wind tunnel test.

The numerical calculation results of the CC-E0020EJ airfoil are compared with the simulation and experimental results of other researchers[29] to verify that the pressure

distribution on the airfoil surface is consistent with the flow. While experimental comparison correction method with angle of attack correction is adopted, the pressure distribution on the surface of CC-E0020EJ airfoil with C_μ=0.047 is presented in Fig. 3. The figure shows that the suction peak at the leading edge and the upper and lower airfoil surfaces can highly match the experimentally obtained pressure coefficients, while the Coanda surface at the trailing edge shows a flow field distribution similar to that of other researchers, indicating that the calculated results can reflect the distribution of the flow field around the airfoil.

In summary, the computational method is able to achieve the computational accuracy and physical phenomena needed in this paper.

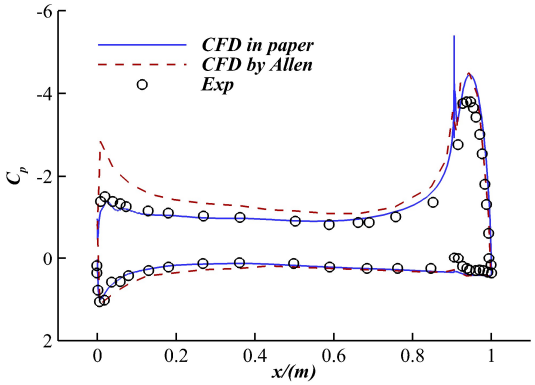

Fig. 3. Comparison of pressure coefficients distribution between numerical simulation and wind tunnel test.

3 Airfoils and Morphing Strategy

The effect of secondary jets on wing flow control has always been a hot research topic in aircraft design. The Coanda surface at the trailing edge of the wing is designed by trimming, and the Coanda effect formed by the additional jet nozzles at the trailing edge improves the circulation about foils, so as to achieve the effect of increasing lift and reducing drag. The jet nozzle position and nozzle height are the two most important basic parameters, and the Coanda circulation control trailing edge trimming scheme has been fully explained by other researchers. The effect of the airfoil geometry itself on the trailing edge jet is not yet known and will be investigated in this paper.

3.1 CCW Modeling

When a large aircraft takes off, it needs a larger lift coefficient as well as lift-to-drag ratio to increase the aircraft climb gradient and reduce the engine thrust, so the optimization objectives of this paper are lift coefficient and lift-to-drag ratio. Under the low-speed flight conditions of the aircraft, three different thicknesses and curvatures of circulation control airfoils are numerically analyzed. In this paper, NASA LS(1)-0417,

also known as GA(W)-1 airfoil, is selected as the baseline geometry of General Aviation Circulation Control Airfoil (GACC). Due to its blunt leading edge and large thickness ratio integration characteristics, it possesses the potential to be applied for active flow control of transonic vehicles.CC-E0020EJ is a standard circulation control airfoil that is widely used for mechanistic studies of circulation control techniques due to its blunt trailing edge characteristics leading to make it easier to observe Coanda attachment effects. In the previous study, our lab completed the modification of the upper and lower nozzles based on the classic NACA0012 airfoil, named as NACA0012-CC circulation control airfoil, and intercepted part of the data as a source of comparative study. Table 1. illustrates the incoming flow conditions of the three-circulation control airfoils and analyzes the lift-to-drag ratios within a certain range of the lift coefficients. It should be noted that the lift-to-drag ratio here is the ratio of lift to effective drag, which is the projection of the force on the airfoil surface in the X-axis plus the thrust coefficient of the jet nozzle in the X-axis direction, so as to avoid a zero-drag coefficient or a negative number. The lift-to-drag ratio curves plotted here do not necessarily represent the flight envelope of maximum efficiency.

Table 1. Incoming flow parameter setting and calculation working conditions.

Airfoil	Mach	Reynolds number	Temperature	C_μ（in figure）
GACC	0.08738	500000	293.15	0.01
CC-E0020EJ	0.08360	1895000	294.10	0.04
NACA0012-CC	0.08360	1895000	294.10	0.02

$$\frac{C_l^*}{C_d} = \frac{C_L - C_T \sin\ _{jet}}{C_D + C_T \cos\theta_{jet}} \tag{4}$$

$$C_T = \frac{\int_{A_j} \frac{1}{2}\rho u_j^2 dA}{\frac{1}{2}\rho_\infty v_\infty^2 C} \tag{5}$$

The aerodynamic performance of the airfoils is investigated based on the thrust-drag decomposition method, and the Mach number cloud and streamline distribution of the three configurations, GACC Airfoil, CC-E0020EJ Airfoil and NACA0012-CC Airfoil, are plotted in Fig. 4. and the range of the achievable lift-to-drag ratios is plotted within their lift coefficient range. Since the three airfoil configurations did not complete their calculations under the same flight conditions and were not in the optimal flight condition at the design point, it is not very meaningful to study the absolute values of the values, but rather to analyze the trends and distributions. In Fig.4(a)(b)(c), it can be observed that although the airfoil geometries are different, the high-speed jets all produce a significant wall attachment effect on the Coanda surface at the trailing edge, which controls the location of the separation point by controlling the jet strength and increases the airfoil circulation thus increasing the lift-to-drag ratio. Compared with the symmetric airfoil (Fig.4(a)), the GACC airfoil undergoes a larger deflection at a smaller

momentum coefficient, which is judged to be caused by the downward bending of the trailing edge of the airfoil itself. As the GACC airfoil is affected by its own curvature, the range of lift coefficient is narrower, while the lift-to-drag ratio is at a relatively high level between 35-60, with a better overall performance. Comparing the two symmetric airfoils CC-E0020EJ and NACA0012-CC, the CC-E0020EJ airfoil with 20% *c* thickness (Fig.4(b)(c)) has a very significant effect on the trailing edge separation vortex suppression, although the deflection degree is not as good as that of the NACA0012-CC airfoil with 12% *c* thickness. In Fig. 4.(d), it is shown that the NACA0012-CC airfoil reaches its maximum lift-to-drag ratio at a lift coefficient of 1.23, the GACC airfoil reaches its maximum at a lift coefficient of 1.45, and the maximum lift-to-drag ratio of the NACA0012-CC airfoil continues to increase until it reaches a lift coefficient of 1.98, until it reaches its peak and then decreases rapidly. Comparing the lift-to-drag ratio ranges of the airfoils with different thicknesses, the CC-E0020EJ airfoil shows good lift-to-drag ratio characteristics in the range of very high lift coefficients, while the NACA0012-CC airfoil deteriorates the lift-to-drag characteristics in the high lift condition. It can be seen that the thin airfoil performs better when the effective lift coefficient is small, which can realize the lift increasing when the aircraft is cruising; the thick airfoil performs better in the range of larger lift coefficients, which is more capable of providing great lift coefficients in the takeoff stage, thus realizing fast takeoff and landing. Observing the GACC airfoils, it can be seen that they show a large lift-to-drag ratio in the range of calculated lift coefficients in this paper, ranging from 37.5 to 59.6; before the lift coefficient reaches 1.45, the lift-to-drag ratio increases steadily; after reaching the maximum lift-to-drag ratio of 59.6, the ratio decreases slowly, and stays at about 54 in the range of lift coefficients from 1.96 to 2.50; when the lift coefficient is as high as 3.27, the lift-to-drag ratio still remains at a high level of 49.5. It shows that although the maximum lift-to-drag ratio of the curved airfoil is lower than that of the two symmetrical airfoils, within the range of achievable lift coefficients, the change of the lift-to-drag ratio is more gentle, and the overall performance is better as it is within the range of higher lift-to-drag ratios.

Comprehensively, the symmetric airfoils with different thicknesses can realize a large lift coefficient increase at 0° angle of approach.On the one hand, the lift-to-drag ratios of NACA0012-CC and CC-E0020EJ airfoil fall back quickly when the lift coefficients reach 1.23 and 1.98 respectively, with little difference in the decay rate, which indicates that the larger momentum coefficients do not guarantee the better lift-to-drag characteristics. On the other hand, in the supercritical airfoil with curvature, the lift-to-drag ratio increases dramatically with the increase of the lift coefficient, and reaches the maximum value when the lift coefficient is 1.45, and then the lift-to-drag ratio decreases slowly, which is more consistent with the requirement of the stability of linear maneuvering, and the supercritical airfoil with curvature is more in line with the selection of airfoils for loop control in the actual flight conditions.

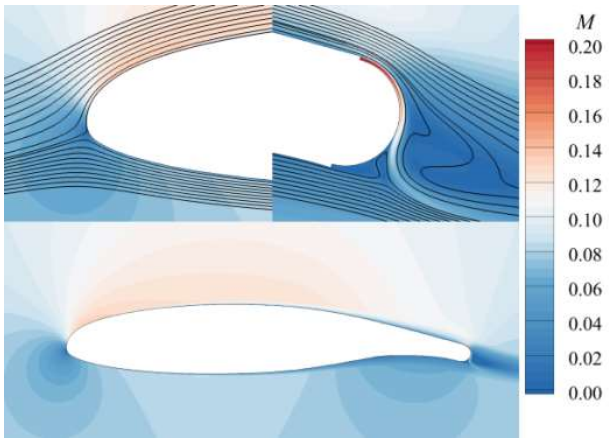

(a) GACC Airfoil

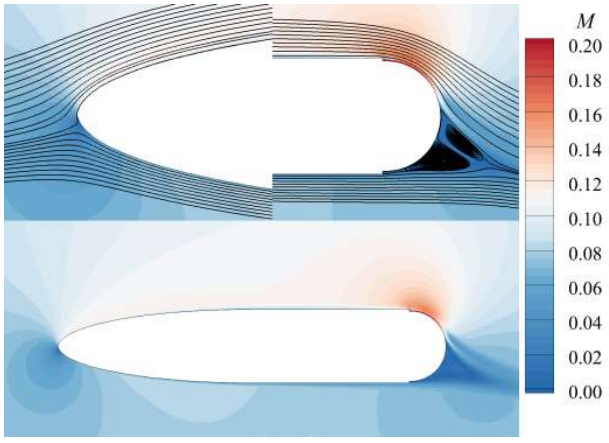

(b) CC-E0020EJ Airfoil

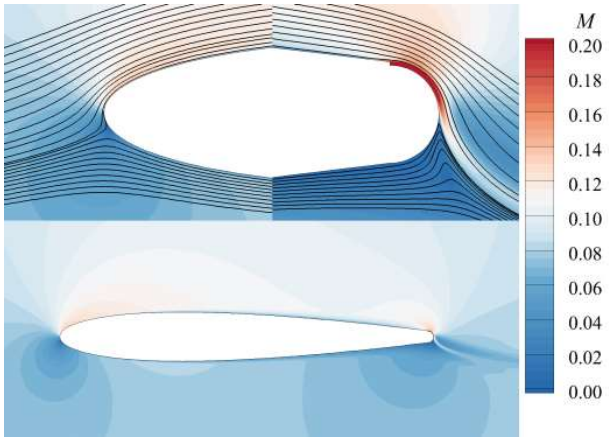

(c) NACA0012-CC Airfoil

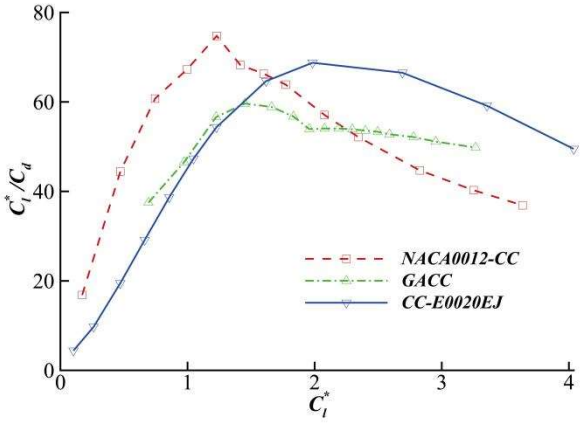

(d) Equivalent lift-drag ratio

Fig. 4. Mach number cloud map and flow line distribution and lift-drag characteristics

3.2 Equivalent Camber

The aerodynamic flaps formed by the high-speed jet separating from the trailing edge of the wing can change the equivalent curvature of the wing, causing the forward stationary point to move backward and the trailing edge separation point to move downward on the curved surface, which creates a control effect similar to that of a variable curvature airfoil. The trailing edge jet sucks up a large amount of ambient incoming flow on the Coanda surface, and the separated trailing edge forms a shape similar to that of a mechanically movable flap, which is also used to control the attitude of the vehicle through the deflection of the aerodynamic flaps.

Fig. 5. shows the pressure distribution of CC-E0020EJ and GACC airfoils under different jet flow coefficient conditions. It can be seen that the pressure coefficient distributions of the upper and lower airfoils of the CC-E0020EJ original configuration are exactly coincident when there is no jet flow, which is the standard flow case of a symmetric airfoil at 0° headway angle. When C_μ=0.01, the pressure coefficient on the upper airfoil decreases, the pressure coefficient on the lower airfoil increases, and the trailing edge pressure coefficient peaks at the blunt trailing edge. Comparing the pressure coefficient distribution of the no-jet case, it can be seen that most of the lift coefficient enhancement at this point is provided by the trailing edge jet and the leading-edge suction peak. When C_μ=0.02~0.03, the leading edge suction peak further increases, and only the intensity of the trailing edge jet increases, which makes the pressure coefficient distributions of both the upper and lower airfoils change greatly, and the range of the trailing edge suction peak expands as well.

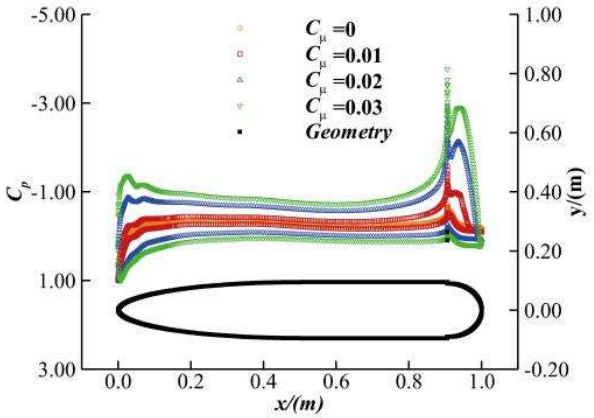

(a) CC-E0020EJ Airfoil

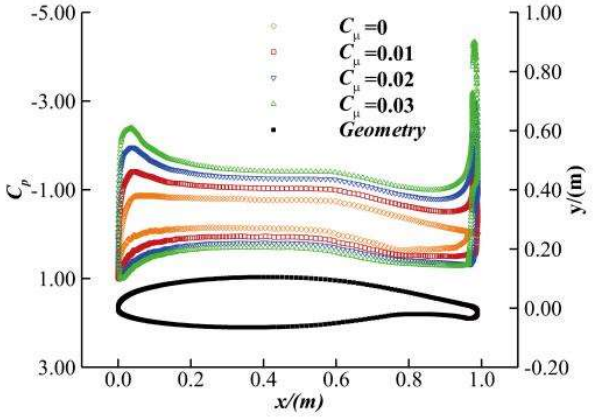

(b) GACC Airfoil

Fig. 5. Surface pressure distribution of CC-E0020EJ and GACC airfoil with different jet momentum coefficients

Comparing the shape of the suction peak at the leading edge, it can be seen that the shape of the aerodynamic flaps at the trailing edge also affects the leading edge of the airfoil, which makes the symmetric airfoil show the pressure coefficient distribution characteristic of the airfoil with curvature. Observing the pressure coefficient change of the GACC airfoil, since the airfoil is a supercritical airfoil modified into an airfoil with curvature, it still shows different pressure distributions on the upper and lower airfoils under the no-jet condition, and at the trailing edge at this time, the pressure distributions gradually converge and tend to the ambient pressure. While at C_μ=0.01, the GACC airfoil also shows an increase in the suction peak at the leading edge, which indicates that the aerodynamic flaps lead to an increase in the equivalent curvature of the airfoil in different configurations. In addition, the difference between the upper and lower airfoil pressures suddenly increases due to the high-speed jet at the trailing edge, and the suction peak is reached rapidly at the jet exit, and the pressure coefficient falls

back rapidly with the jet deflection caused by the Coanda effect. The further increase of the jet flow coefficient makes the pressure difference between the upper and lower airfoils increase continuously according to the same regular trend when C_μ reaches 0.02-0.03, which is equivalent to changing the geometrical configuration of the airfoil and forming a virtual rudder.

3.3 Jet Deflection

In the study of the previous subsection, the airfoils with curvature and the symmetric airfoils have another important geometric parameter, i.e., the angle between the jet exit and the horizontal incoming velocity, in addition to the difference in thickness and curvature. In order to exclude the influence of the upper and lower airfoils and leading edges of the airfoil itself, Fig. 6. shows the GACC airfoil with a 19° deflection angle modified in this paper from the 15° jet exit deflection angle in the previous section, which is basically a downward deflection of only 4° for the trailing edge and 70% of the lower airfoil at 70% *c*.

Fig. 7. elucidates the effect of different nozzle angles on the lift coefficient and pitching moment. The important concept in the circulation control is the critical momentum coefficient and is divided into the separation control phase and the super-circulation control phase. In the separation control stage, C_l shows a linear growth trend with the increase of C_μ, and the efficiency of the jet's lift and drag reduction becomes lower in the super-circulation control stage, and C_l is positively correlated with the arithmetic square root of C_μ, which deviates from the linear trend. It can be observed in the figure that both configurations reach the transition stage from the separation control to the super-circulation control stage near C_μ=0.02. At C_μ = 0.03, the two lift coefficients produce a slight difference, and the slope of the C_μ-C_l curve for the configuration with a jet deflection angle of 19° is smaller thereafter, indicating that the transition stage is slightly delayed compared to the base configuration with a 15° deflection. The variation of pitching moment with lift coefficient is observed from the C_l-C_m curves, which are almost identical when the same lift coefficient is reached. To summarize, in the case where the trailing edge jet dominates the aerodynamic flap deflection on the Coanda surface, the differences in aerodynamic parameters during the separation control phase are very small, and increasing the jet exit angle delays the transition of the super-circulation control phase, and the jet exit angle does not seriously affect the aerodynamic performance of the wing in the same curvature-based geometrical configuration. In conclusion, it can be seen that compared with the equivalent curvature increase caused by the aerodynamic flap, the geometric curvature increase caused by the trailing edge deflection angle has a relatively small effect on the overall aerodynamic characteristics of the airfoil.

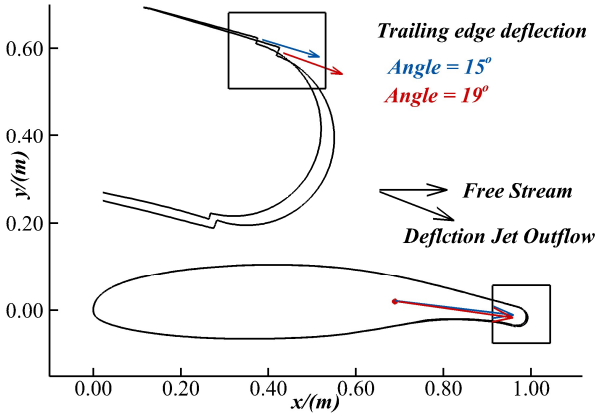

Fig. 6. GACC airfoil configuration with 15° and 19° jet deflection Angle

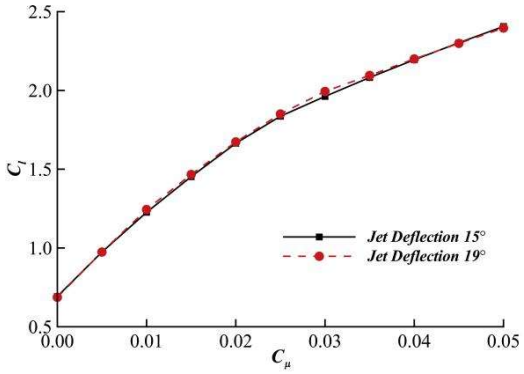

(a) Lift coefficient characteristic

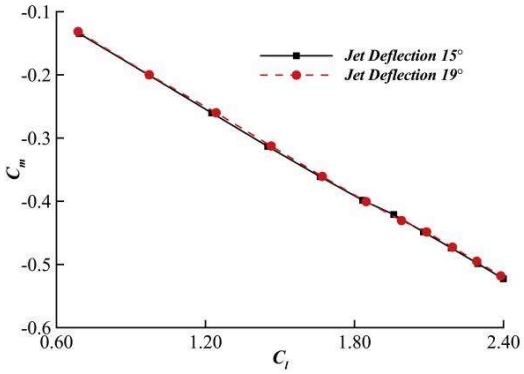

(b) Pitching moment characteristics

Fig. 7. Aerodynamic characteristics of GACC airfoil with 15° and 19° jet deflection Angle

4 Numerical Analysis of Wing Models

Typical aircraft speeds at takeoff or landing are Mach 0.3, and large aspect ratio aircraft operate at relatively low cruise speeds with a severe lack of maneuverability. Airfoils for civil aviation usually have a chord ratio greater than 8. The larger the chord ratio, the lower the induced drag for the same area, and the smaller the effect of wingtip vortices on the flow regime. However, the vortex structure on the airfoil will interfere with the trailing edge jet, but it is unwise to increase the chord ratio to improve the aerodynamic characteristics of circulation control. Exploring and avoiding the negative effects of wingtip vortices is the focus of the next research in this paper.

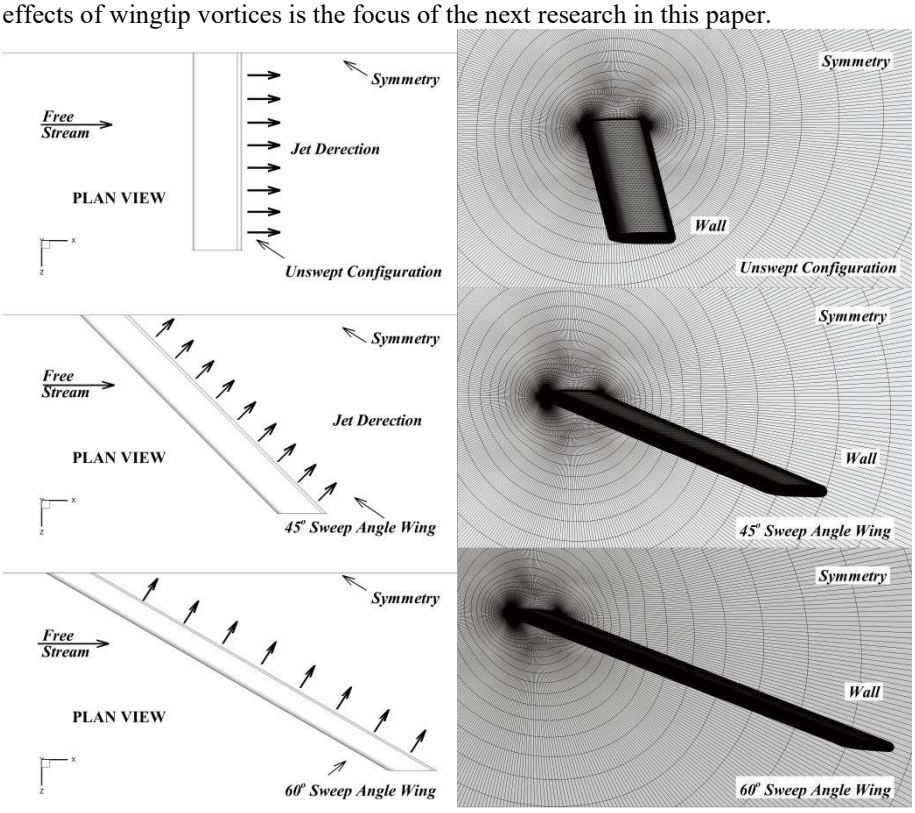

Fig. 8. Configuration and mesh of straight wing and swept wing

For this study, a spreading ratio of λ=8 was chosen as the geometrical parameter for the flat wing, and the computational states were Mach number *Ma*=0.3, *Re*=6.9865×10^6 and T=288.15K. It was concluded in the research[30] that the jet perpendicular to the trailing edge has a greater impact on aerodynamic loads, including the increasing lift, drag, and nose-down moment than the jet in the freestream direction. So the velocity outlet of trailing edge nozzle is adopted to flow out perpendicularly with the jet nozzle, on the basis of which a reasonably designed jet nozzle position is investigated to achieve better control. Fig. 8. shows the structured mesh near the airfoil configuration

and the object surface designed in this paper in the 3-D study, and the boundary conditions of each part are indicated in the figure.

4.1 Flat Wing Performance under Wingtip Vortex Interference

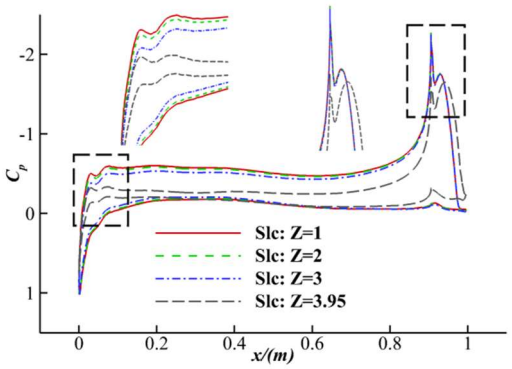

(a) α=0° , U_{jet}=200m/s, x-y plane

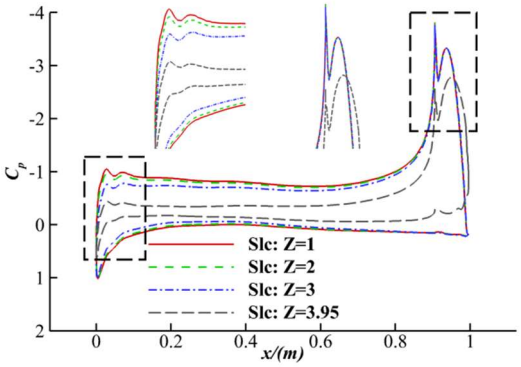

(b) α=0° , U_{jet}=300m/s, x-y plane

Fig. 9. Pressure distribution on the z/c=1, z/c=2, z/c=3, z/c=3.95 cross section

Fig. 9. shows the distribution of pressure coefficients in the x-y plane for different jet exit velocities for the spreading slice projection of the wing in the z-direction. Detailed plots of the leading-edge suction peak as well as the trailing edge jet suction peak are shown in the black dashed box. In the z/c=3.95 cross-section near the wingtip, comparing the 54.03% surface pressure loss in the z/c=1 cross-section, the suction peak at the leading edge decreases substantially, the pressure difference between the upper and lower airfoil surfaces decreases, and the suction peak of the trailing edge jet decreases in peak value and the position of the suction peak is shifted backward. Observing the pressure coefficient losses at different cross sections, 12.77% pressure loss still exists on the upper and lower surfaces of the z/c=3 cross section compared to the z/c=1 cross section, but it has shown the same distribution pattern; the pressure loss on the z/c=2

cross section has been reduced to a sufficiently small level of 3.46%.In the z/c=3 section, the pressure distribution curves of the trailing edge jet in the region after x/c reaches 0.8 almost completely overlap, indicating that at this time, although the leading edge of the wing is still interfered by the wingtip vortex, the trailing edge jet has been able to achieve a good enough control effect. The above law still holds for two different jet intensities. Further comparing U_{jet}=200m/s and U_{jet}=300m/s jet velocity increase, 54.03% and 57.36% are lost in z/c=3.95 cross section, 12.77% are lost in both z/c=3 cross section and 3.46% and 3.50% are lost in z/c=2 cross section, respectively. The interference of the wingtip vortices on the trailing edge jet are all reduced to a sufficiently small level at the z/c=3 cross section. However, as the jet strength increases, the difference between the upper and lower airfoils at the same cross-section increases, and the presence of wingtip vortices prevents the trailing-edge jet from achieving the uplift effect that it would have had if the flow had been stabilized.

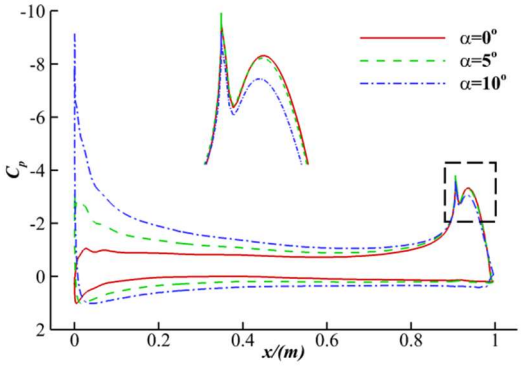

Fig. 10. α=0°, 5°, 10°, U_{jet}=300m/s, pressure distribution on the z/c=1 cross section

Fig. 10. shows the range of influence of different angles of approach on the distribution of pressure coefficients at z/c=1 at the root of the wing. From Fig. 9. it can be seen that the flow at the z/c=1 interface at the root of the wing is not disturbed at all by the wingtip vortices, so the effect of the flight angle of approach on the trailing edge jet on the 3D wing is considered purely in this cross-section. The difference in the suction peak at the leading edge is entirely due to the incoming flow headings, so only the effects on the Coanda trailing edge at the wing chordal distances of x/c=0.9~1 are compared for the α=0°, 5°, 10° headings. At α=0°, incoming flow velocity is in the same direction as the jet velocity, and the increase in lift coefficients at α=5° and 10° is observed. Comparing the cross-section increase in lift coefficients, it can be seen that compared with the flow field distribution at α=0°, the uplift coefficients at α=5° and 10° increase by 44.31% and 91.54%, and the increase in uplift coefficients mainly comes from the increase of the suction peak at the leading edge. At α=5°, the pressure coefficient distribution in the enlarged diagram overlaps at α=0°, and as the angle of attack increases to α=10°, the pressure coefficient at the exit of the jet nozzle is basically unchanged, while the suction peak on the surface of Coanda at the trailing edge decreases. From this, it can be concluded that the incoming angle of attack has less influence on the attachment effect of Coanda surface at the trailing edge at a smaller angle of attack.

The wing angle of approach is directly related to the strength of wingtip vortex, the larger the angle of approach, the larger the pressure difference between the upper and lower surfaces of the wing, and the larger the amount of wingtip vortex. In order to more intuitively analyze the influence range of wingtip vortices under the complete distribution of trailing edge jets, Fig. 11. plots the pressure clouds and streamline distributions on the upper surface and wingtips of the wing for different incoming jet angles at different jet velocities. Firstly, comparing the different jet velocity conditions, the flow line washing phenomenon at the trailing edge of the wing at U_{jet}=300m/s is extremely significant, the wing tip vortices flow more complicated in the wake area of the wing trailing edge, and the trailing edge jet aggravates the fragmentation of the wing tip vortices and enlarges the influence range of the wake.

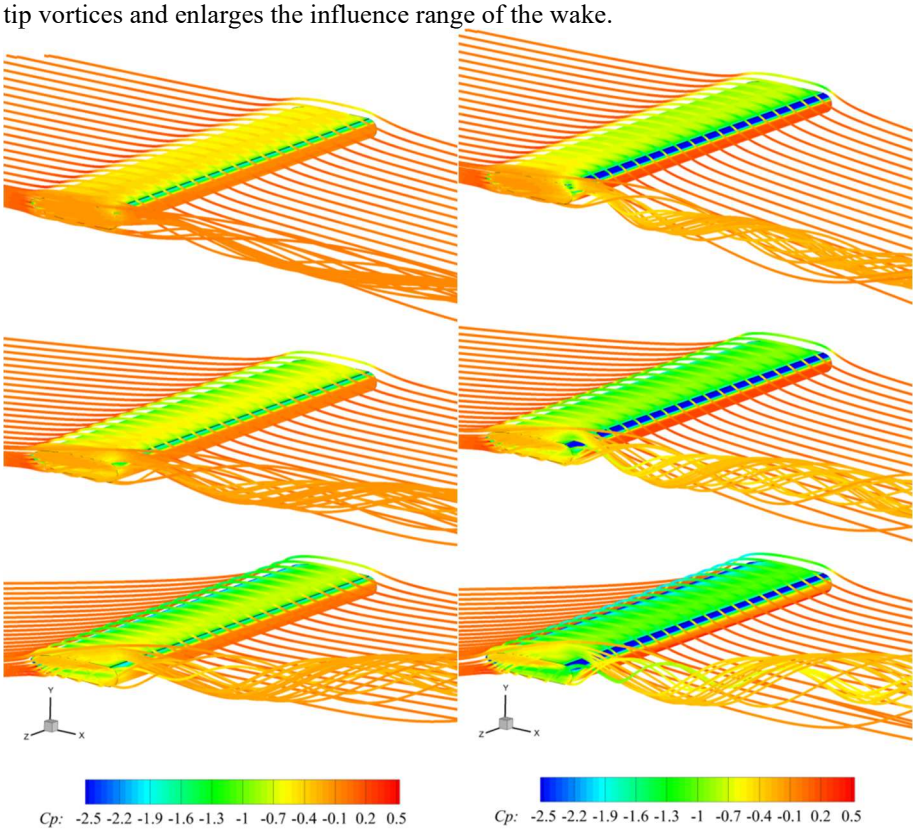

(a) U_{jet}=200m/s (b) U_{jet}=300m/s

Fig. 11. Pressure distribution and streamline at 0°, 5°, 10° angles of attack

Comparison of the surface pressure coefficient maps shows that the pressure coefficient in the jet attachment region decreases, while the pressure coefficient in the detachment region is increased by the aerodynamic flap downwash, forming a high-pressure region on the Coanda surface. Secondly, comparing the flow under different head-

way angles, the downwash effect of the trailing edge jet remains significant as the headway angle increases. The pressure of the lower airfoil increases and the pressure of the upper airfoil decreases, which makes the downwash effect of the lower airfoil more significant and the suction effect of the upper airfoil more significant. To a certain extent, the trailing edge jet can eliminate the interference of the wing tip vortex on the upper airfoil of the wing, but such a suppression effect is limited. Areas of trailing edge jet failure due to wingtip vortices still exist, and the extent of the "dead zone" needs to be explored qualitatively and controlled.

Generally, the secondary jet interferes with the aircraft wake flow field, prompting the aircraft wingtip vortex to dissipate the energy in advance, and the important prerequisite for the effective implementation of the active flow control technology is to accurately obtain the characteristics of the wingtip vortex wake flow field. At the same time, multi-parameter and multi-objective optimization should be considered in the design stage, including the selection of jet coefficient, jet direction, nozzle shape and nozzle position. To achieve the vortex control of the aircraft, it is necessary to accurately know the flow structure in the wake vortex and then intervene and optimize it. The focus of this paper is on the exploration of the effective working range of circulation control technology, the layout design for the region less affected by the wingtip vortex, and the avoidance of wingtip vortex interference to improve the computational efficiency of the numerical simulation in the pre-design stage.

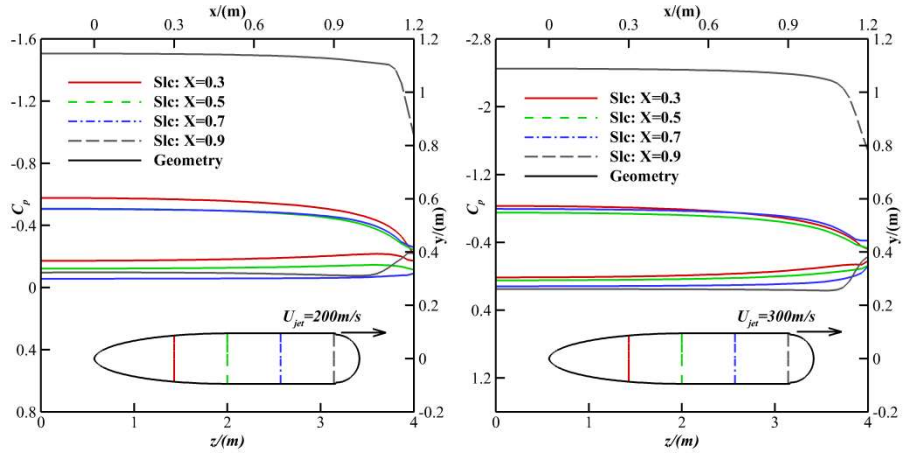

(a) U_{jet}=200m/s (b) U_{jet}=300m/s

Fig. 12. U_{jet} =200m/s, U_{jet}=300m/s, pressure distribution on the x/c=0.3, x/c=0.5, x/c=0.7, x/c=0.9 cross section

Fig. 12. shows the pressure distribution on each section of the wing in the chordwise direction, so as to observe the range of influence of the wing tip vortex on the upper and lower airfoils in the spreading direction. At U_{jet}=200m/s, the pressure coefficients of the wing x/c=0.3, x/c=0.5, x/c=0.7 cross sections are mainly concentrated in the range of z/c=3.5~4. x/c=0.9 cross section is the region of the interaction between the wingtip vortex and trailing-edge jet, and the pressure coefficients of the upper airfoil at the spreading position of z/c=3.7 recover rapidly under the effect of the high-velocity jet

and smooth in the region of z/c=3, which is the region of the upper airfoil. The pressure coefficient of the upper airfoil at z/c=3.7 is rapidly recovered and smoothed out at z/c=3, and the lower airfoil reaches flow stabilization at z/c=3.5 section. The same trend is shown at U_{jet}=300m/s, which indicates that the design of jet outlet is avoided at least at z/c=3.5~4 on the studied configuration in this paper, and the design of circulation control technique in the range of z/c less than 3 will avoid the wingtip vortex interference to a large extent.

4.2 Pitching-Moment Performance under Sweep Angle Interference

The backswept angles χ_0=45° and χ_0=60° are selected and Fig. 8. demonstrates the design scheme for uniform and complete distribution of trailing edge jets on the wing with different backswept angles. Due to the sensitivity of the secondary jets to the wing configuration and the ambient incoming flow, it is necessary to explore the influence of the three-dimensional effects on large spreading ratio layouts, in addition to investigating the regularity mechanism on two-dimensional airfoils and flat wings.

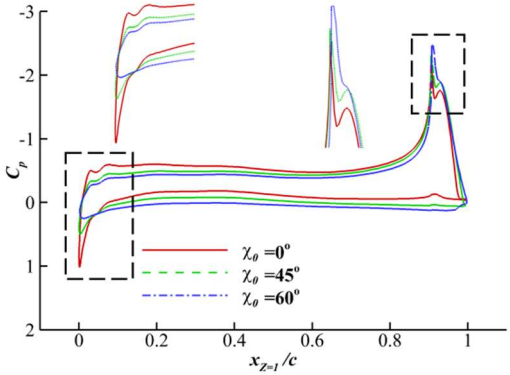

Fig. 13. The pressure coefficient distribution on the Z=1 section at the velocity outlet 200m/s at the sweep Angle χ_0=0°, χ_0=45°, χ_0=60°

Fig. 13. plots the pressure distribution on the surface of the airfoil for the same trailing edge jet velocity for a flat and swept airfoil at z/c=1 wing root cross section. Taking χ_0=0° flat wing as the benchmark, examining the aerodynamic characteristics of the wing root cross-section, it can be seen that there are 5.95% and 8.87% lift coefficient growth on the χ_0=45° and χ_0=60° swept back wing cross-section, respectively. Observing the pressure distribution law, the larger the wing swept back angle, the smaller the suction peak at the leading edge of the wing. The pressure coefficients at the upper airfoil surface and at the stationing point decrease, while the high-pressure region at the lower airfoil surface increases. It can be observed that the pressure distribution at the trailing edge of the airfoil, the suction peaks on the Coanda surface continue to increase as the angle of backswing increases. The level of performance at any spreading position on χ_0=0°, χ_0=45°, and χ_0=60° wing sections depend on the three-dimensional effect of the finite airfoil and its variation with the angle of back-sweep.

The pressure clouds and streamline distributions on the upper surface of the wing and the wingtip for different jet velocities for different incoming flow angles are plotted in Fig. 14. On a finite wingspan swept-back wing, the downwash of the wing tip decreases, and the downwash of the wing root increases, and the deviation of the wing root from the wing tip is very intuitively observed in the Fig. At the end of the jet, the jet sheet is torn from the Coanda surface by the wingtip vortex, creating an extremely strong vortex. And because the jet exit velocity is not parallel to the incoming velocity, i.e., the wake of the wingtip vortex detachment forms an angle with the velocity direction of the trailing edge jet. The interaction of these two structures can produce some extremely complex flow fields that empirically appear to be time-varying and periodic. The shedding of these additional strong vortices goes some way to explaining the inconsistency between the analyzed and empirical downwash distributions of a flat wing in a swept-back layout and is of interest for wake prediction and wing or vortex interactions in circulation control wings. It can be seen in the figure that the disruption of the wingtip vortices for circulation control effect stems mainly from the disruption of the downwash interaction, and that the significant difference in the downwash distributions for the wing spread is estimated to be a key factor in explaining the wake effect of any finite airfoil.

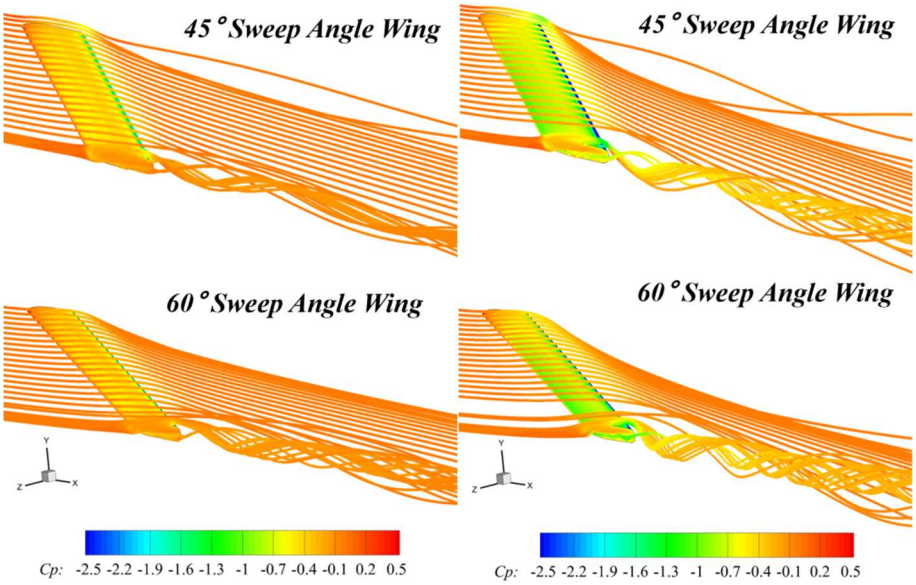

(a) U_{jet}=200m/s (b) U_{jet}=300m/s

Fig. 14. Pressure coefficient distributions and streamlines for wings with 45° and 60° swept-back angles.

5 Conclusion

The research observes the alteration of the upper wing surface pressure distribution due to the Coanda effect, resulting in pitch moments. Consequently, a novel concept of

equivalent camber for aerodynamic flaps is proposed. Numerical simulations and analyses are conducted within this paper to investigate the aerodynamic control effects of symmetric airfoils and airfoils with curvature under varying jet conditions driven by circulation control. Furthermore, the aerodynamic analysis of both straight and swept-wing configurations is integrated. The collective findings yield the following conclusions:

1) Aiming at the problem that the aerodynamic parameter laws of circulation control technology are different on different configuration airfoils, the study of lift coefficient and lift-to-drag ratio is carried out. CC-E0020EJ airfoil shows greater advantages in the observation of Coanda effect, with a wider range of applicable momentum coefficients and larger lift-to-drag ratios; the maximum lift-to-drag ratio is largest in the NACA0012-CC modified airfoil, and lift-to-drag ratio decreases significantly in the case of high lift; GACC supercritical airfoil with curvature has a larger deflection angle to blow out aerodynamic flaps, which limits its lift performance, while its maneuvering torque linearity is better. The NACA0012-CC modified airfoil has the largest maximum lift-to-drag ratio, while the lift-to-drag ratio decreases substantially at high lift; the GACC supercritical airfoil with curvature blows out aerodynamic flaps with a larger deflection angle, which restricts its lift performance, while its maneuvering torque has better linearity.

2) Secondly, we explored the influence range of wingtip vortices on a flat wing with circulation control and found that the vortex structure generated by the wingtip vortices is coupled with the trailing-edge jet. The trailing edge jet accelerates the breakup and decay of the wingtip vortices, and the presence of the wingtip vortices causes the loop volume control technique to be completely ineffective at a distance of z/c=3.95 to the wingtip until it is basically restored at z/c=3.

3) Last but not least, aerodynamic analyses for a large swept-back wing with different swept-back angles show that vortex shedding at the tip of the jet finite end appears to be critical in determining the effectiveness of the localized downwash flow field and circulation control.

The results of this study confirm that the blowing angle of the jet outlet is not as important as expected and that the distribution of the pressure coefficients is mainly influenced by the overall wing configuration and the blowing of the trailing edge flaps. The range of lift coefficients can be adjusted by circulation control technique without changing the attitude of the vehicle, and a wide range of aerodynamic control can be realized within the takeoff and landing range. Trailing edge blown flaps have been shown to be more effective in achieving high lift-to-drag ratios at low flight speeds and improved pitching moment maneuverability than conventional tip-tailed edge airfoils.

References

1. AVIDSON I M. Aerofoil boundary layer control systems:US3062483 A[P]. 1962.
2. J P Fielding and A Mills and H Smith. Design and manufacture of the DEMON unmanned air vehicle demonstrator vehicle[J]. Proceedings of the Institution of Mechanical Engineers, Part G: Journal of Aerospace Engineering, 2010, 224(4): 365-372.

3. Warsop C, Crowther W J, Shearwood T. NATO AVT-239 task group: flight demonstration of fluidic flight controls on the MAGMA subscale demonstrator aircraft [C]. AIAA SciTech Conference, 2019.
4. Warsop C, Crowther W, Forster M. NATO AVT-239 Task Group: Supercritical Coanda based circulation control and fluidic thrust vectoring[C]//AIAA Scitech 2019 Forum. 2019: 0044.
5. Hutchin, C., NATO AVT-239: Control effectiveness and system sizing requirements for integration of fluidic flight controls on the SACCON aircraft configuration[C]//AIAA Scitech 2019 Forum. 2019: 0280.
6. Smith D R, Warsop C. NATO AVT-239 Task Group:'Innovative Control Effectors for Manoeuvring of Air Vehicles'–Introduction and Overview[C]//AIAA Scitech 2019 Forum. 2019: 0041.
7. Wang HY. Research and Flight Testing of Aerodynamic Characteristics for Unmanned Aircraft Based on Circulation Control [D]. Nanjing: Nanjing University of Aeronautics and Astronautics; 2014. (In Chinese)
8. Chen K, Shi Z, Zhu J, et al. Roll aerodynamic characteristics study of an unmanned aerial vehicle based on circulation control technology[J]. Proceedings of the Institution of Mechanical Engineers, Part G: Journal of Aerospace Engineering, 2019, 233(3): 871-882.
9. Sun Q B, Shi Z W, Geng X, Wang L S, Zhang W Y. Attitude Control of Tailless Flying Wing Aircraft Based on Active Flow Control Technology[J]. Acta Aeronautica et Astronautica Sinica, 2020, 41(12): 190-199. (In Chinese)
10. Qu L X, Li Y, Bai X J. Research Progress on Application Validation of Fluid Thrust Vectoring Technology[J]. Aeronautical Science and Technology, 2020, 31(05): 64-72. (In Chinese)
11. Fu Z J, Xu H Y, Du H, Wang Y H, Xu Y. Research on Aerodynamic Characteristics of Virtual Flap Wing Based on Circulation Control[J]. Aeronautical Science and Technology, 2020, 31(05): 11-22. (In Chinese)
12. Zhenbing L U O, Zhijie Z, Jiefu L I U, et al. Novel Roll effector based on zero-mass-flux dual synthetic jets and its flight test[J]. Chinese Journal of Aeronautics, 2021.
13. Zhang W W, Zhai J, Liu X B, et al. Study on Dynamic Load Characteristics of Low-Frequency High-Power Synthetic Jet at Airfoil Trailing Edge—Part B: Analysis of Dynamic Aerodynamic Load Characteristics. Experimental Fluid Mechanics, 2014, 28(5): 24-32. (In Chinese)
14. Liu X B, Zhang W W, Jiang Y W, et al. Numerical Study on the Influence of Trailing-Edge Synthetic Jet on Unsteady Aerodynamic Characteristics of Airfoil[J]. Acta Aerodynamica Sinica, 2012, 30(05): 606-612. (In Chinese)
15. Zhang Z Y, Wang T T, Chen Z H, et al. Effects of Blowing and Suction Jet on Aerodynamic Performance of NACA0012 Airfoil at Low Reynolds Numbers[J]. Acta Aerodynamica Sinica, 2020, 38(01): 58-65. (In Chinese)
16. LI Y J, LUO Z B, DENG X, et al. Experimental investigation on flow separation control of stalled NACA0015 airfoil using dual synthetic jet actuatorlJ7. Acta Aeronautica et Astronautica Sinica, 20 16, 37(3): 817-825.
17. Englar R, Jones G, Allan B, et al. 2-D circulation control airfoil benchmark experiments intended for CFD code validation[C]//47th AIAA Aerospace sciences meeting including the new horizons forum and aerospace exposition. 2009: 902.
18. Li Y, Qin N. Airfoil gust load alleviation by circulation control[J]. Aerospace Science and Technology, 2020, 98: 105622.
19. Han Z H, Song W P, Qiao Z D. Numerical Simulation Study on Active Flow Control of OA212 Airfoil[J]. Acta Aerodynamica Sinica, 2009, 27(06): 639-644. (In Chinese)

20. Bai J Q, Xin L, Liu N, et al. Numerical Simulation of Separation of Distributed Zero-Mass Jet Control Lift Augmentation Device[J]. Journal of Northwestern Polytechnical University, 2014, 32(02): 188-194. (In Chinese)
21. Lei Y C, Zhang D C, Zhang Y H. Unsteady Aerodynamic Force Modeling of Momentum-Controlled Airfoil[J]. Journal of Beijing University of Aeronautics and Astronautics, 2021, 47(10): 2138-2148. DOI: 10.13700/j.bh.1001-5965.2020.0360. (In Chinese)
22. Song Y P, Yang X G, Li Y C, et al. Numerical Simulation of Coanda Effect in Circulation Control Airfoil[J]. Journal of Engineering Thermophysics, 2010, 31(09): 1475-1479. (In Chinese)
23. JIANGYB, ZHANG L, HUANG Y, et al. Lit resoonse characteristics of a circulation control airfoi with internally biown flapi J. Acta Aeronautica et Astronautica Sinica, 2018， 39(7). 121807 (in Chinese). doi:10. 7527/S1000-6893.2017 21807
24. KONG B, WANG F X, ZHOU T. The aerodynamic design of seamlessly camber-variable airfoil based on circulation control Jl. Acta Aerodynamica Sinica，2013，31(5):583-586
25. Jones G, Viken S, Washburn A, et al. An active flow circulation-controlled flap concept for general aviation aircraft applications[C]//1st Flow control conference. 2002: 3157.
26. Zhang Y H, Zhang D C, Hu M Q, et al. Mechanism of Circulation Control on Airfoil Aerodynamic Characteristics[J]. Journal of Air Force Engineering University (Natural Science Edition), 2015, 16(01): 10-13. (In Chinese)
27. Hoholis G. Assessment of fluidic control effectors using computational fluid dynamics[M]. The University of Liverpool (United Kingdom), 2016.
28. Jones G S. Pneumatic Flap Performance for a 2D Circulation Control Airfoil, Steady and Pulsed[C]. Proceedings of the 2004 NASA/ONR Circulation Control Workshop, Part 2. 2005.
29. Allan B, Jones G, Lin J. Reynolds-averaged navier-stokes simulation of a 2-D circulation control wind tunnel experiment[C]//49th AIAA Aerospace sciences meeting including the new horizons forum and aerospace exposition. 2011: 25.
30. Shao S, Guo Z, Hou Z, et al. Effects of Coanda jet direction on the aerodynamics and flow physics of the swept circulation control wing[J]. Proceedings of the Institution of Mechanical Engineers, Part G: Journal of Aerospace Engineering, 2022, 236(13): 2633-2654.